

Synthesis, Structure and Density Functional Theory (DFT) Study of a Rhenium(I) Pyridylpyrazol Complex as a Potential Photocatalyst for CO₂ Reduction

(Sintesis, Struktur dan Kajian Teori Fungsi Ketumpatan (DFT) ke atas Kompleks Rhenium(I) Piridilpirazol sebagai Fotomangkin untuk Penurunan CO₂)

WUN FUI MARK-LEE, YAN YI CHONG, KUNG PUI LAW, ISHAK B. AHMAD & MOHAMMAD B. KASSIM*

ABSTRACT

The Re(I) complex, [Re(PyPzH)(CO)₃Cl] where PyPzH = 2-(1H-pyrazol-3-yl)pyridine, was successfully synthesised and characterised with an infrared (IR), ultraviolet-visible (UV-Vis), ¹H and ¹³C nuclear magnetic resonance (NMR) spectroscopies and X-ray crystallography. The IR spectrum featured three ν(C≡O), ν(N-H), ν(C=N) and ν(C=C) signals at (1860-2020), 3137, 1614 and 1513 cm⁻¹, respectively. The UV-Vis spectrum of the complex exhibited ligand-centred (π@>*) electronic excitations [$\lambda_{max} = 227$ nm, $\epsilon = 1.942 \times 10^4$ M⁻¹cm⁻¹; $\lambda_{max} = 292$ nm, $\epsilon = 0.853 \times 10^4$ M⁻¹cm⁻¹] and a metal-to-ligand charge transfer (MLCT) band [$\lambda_{max} = 331$ nm, $\epsilon = 0.467 \times 10^4$ M⁻¹cm⁻¹]. The ¹³C and ¹H-NMR spectra exhibited the characteristic signals of the three C≡O (189.0 – 199.0 ppm) and NH (14.84 ppm), respectively. The X-ray structure of [Re(PyPzH)(CO)₃Cl] showed the crystal adopted a monoclinic system with a C2/c space group [unit cell dimensions: $a = 27.7422(14)$ Å, $b = 11.1456(5)$ Å, $c = 9.2461(4)$ Å with $\alpha = \gamma = 90^\circ$ and $\beta = 92.552(2)^\circ$]. Density functional theory (DFT) and time-dependent (TD) DFT calculations were performed to investigate the optimised structural geometry and electronic properties of the title complex. The results showed that the highest-occupied molecular orbital (HOMO) was predominantly found on the dπ-orbitals of Re(I), Cl and CO. While the lowest-unoccupied molecular orbital (LUMO) was located on the PyPzH moiety. The structural and photophysical properties of the [Re(PyPzH)(CO)₃Cl] were established and the reaction enthalpies for the dissociation of Cl atom in the formation of [Re(PyPzH)(CO)₃]^{*} were discussed in view of its potential application for photocatalytic CO₂ reduction.

Keywords: Crystal structure; DFT; photocatalytic CO₂ reduction; pyridylpyrazole; rhenium(I) polypyridine

ABSTRAK

Kompleks Re(I) [Re(PyPzH)(CO)₃Cl] dengan PyPzH = 2-(1H-pirazol-3-il)piridina telah berjaya disintesis dan dicirikan dengan spektroskopi inframerah (IR), ultralembayung-nampak (UV-Vis) dan resonans magnet nukleus (RMN) ¹³C dan ¹H dan kristalografi sinar-X. Spektrum inframerah menunjukkan kehadiran tiga jalur ν(C≡O), ν(N-H), ν(C=N) dan ν(C=C) masing-masing pada (1860-2020), 3137, 1614 dan 1513 cm⁻¹. Spektrum UV-Vis kompleks menunjukkan peralihan elektronik berpusatkan ligan (π@>*) [$\lambda_{maks} = 227$ nm, $\epsilon = 1.942 \times 10^4$ M⁻¹cm⁻¹; $\lambda_{maks} = 292$ nm, $\epsilon = 0.853 \times 10^4$ M⁻¹cm⁻¹] dan satu jalur peralihan caj logam kepada ligan (MLCT) [$\lambda_{maks} = 331$ nm, $\epsilon = 0.467 \times 10^4$ M⁻¹cm⁻¹]. Spektrum RMN ¹³C dan ¹H masing-masing menunjukkan isyarat cirian untuk tiga isyarat kumpulan C≡O (189.0 - 199.0 ppm) dan NH (14.84 ppm). Struktur X-ray bagi hablur tunggal [Re(PyPzH)(CO)₃Cl] memberikan sistem monoklinik dengan kumpulan ruang C2/c dengan dimensi sel unit sel $a = 27.7422(14)$ Å, $b = 11.1456(5)$ Å, $c = 9.2461(4)$ Å dengan $\alpha = \gamma = 90^\circ$ dan $\beta = 92.552(2)^\circ$. Pengiraan berdasarkan teori fungsi ketumpatan (DFT) dan DFT bersandar masa (TD) telah dijalankan untuk membangunkan struktur geometri optimum dan ciri elektronik kompleks [Re(PyPzH)(CO)₃Cl]. Keputusan kajian menunjukkan orbital molekul terisi dengan tenaga tertinggi (HOMO) disetempatan pada orbital-dπ Re(I), Cl dan CO manakala orbital molekul tidak terisi dengan tenaga terendah (LUMO) terletak pada moiety PyPzH. Struktur dan sifat fotofizikal kompleks [Re(PyPzH)(CO)₃Cl] telah dikenal pasti dan entalpi tindak balas untuk penguraian atom Cl untuk pembentukan [Re(PyPzH)(CO)₃]^{*} juga dibincangkan untuk aplikasi sebagai fotomangkin penurunan CO₂ yang berpotensi.

Kata kunci: DFT; fotomangkin penurunan CO₂; piridilpirazol; renium(I) polipiridina; struktur kristal

INTRODUCTION

The use of fossil fuel energy to spur modern civilisation has inadvertently increased the concentration of carbon dioxide in our atmosphere which imminently causes global warming due to the greenhouse effect. Two promising practices are being intensively studied to circumvent the

disastrous effect of fossil fuel consumption. One of the sensible approaches was to capture the emitted CO₂ and then utilise it as a feedstock for the production of other raw materials and renewable fuels such as formic acid, methane and methanol (Komala & Khun 2014; Radaideh et al. 2016; Tamaki & Ishitani 2017). The other approach, which

is not the interest of this paper, is to produce hydrogen as an alternative green-fuel to overcome problems of a hydrocarbon combustion since the burning of hydrogen gas only produces water as a side product (Ng et al. 2018, 2017, 2012; Yilmaz et al. 2016).

One of the reported means to utilise CO_2 is by photocatalytic reduction pathway (Yamazaki et al. 2015). Typically, metal complexes are used in the reduction of CO_2 with relatively high quantum yields and selectivity. In 1983, Hawecker et al. has reported the efficient use of rhenium(I) tricarbonyl complexes namely $[\text{Re}(\text{bpy})(\text{CO})_3(\text{L})]$ (bpy = 2,2'-bipyridine, L = Cl and Br) in the photocatalytic reduction of CO_2 . These Re(I) complexes have since used as a benchmark for further structural modification to improve its catalytic activity. Several structural designs have been employed which focuses on either the substitution of axial L ligand with other groups or the implementation of ancillary extensions on the bpy ligand (Doherty et al. 2009; Gibson & He 2001; Yamazaki et al. 2015). In the CO_2 reductive cycle, the first step involves the formation of one-electron reduction species (OERS) of Re^{II} with the subsequent dissociation of L ligand from the Re metal centre (Agarwal et al. 2011; Sahara & Ishitani 2015).

In this study, we propose a derivative of a Re(I) tricarbonyl complex with the 2-(pyrazol-3-yl)pyridine (PyPzH) diimine ligand in which the PyPzH ligand consist of a five-membered heterocycle pyrazole (strong σ donor) and a six-membered heterocycle pyridine (π acceptor) moieties. This may cause a synergistic effect on the electron distribution where the electron density is delocalised from the pyrazole group to the metal ion and then return the electrons density back to the pyridine group that essentially enhances the stability of the five-membered ring metal chelate generated from the formation of the coordination complex (Chou & Chi 2006). Herein, the synthesis, characterisation and photophysical properties of the title compound will be established. Furthermore, a preliminary investigation on the complex's potential to act as a photocatalyst for CO_2 reduction was carried out through the investigation of enthalpies involved in the chloride dissociation to form a $[\text{Re}(\text{PyPzH})(\text{CO})_3]'$, which is an important species in the photocatalytic cycle.

EXPERIMENTAL DETAILS

SYNTHESIS OF $[\text{Re}(\text{PyPzH})(\text{CO})_3\text{Cl}]$ COMPLEX

The 2-(1H-pyrazol-3-yl)pyridine compound or PyPzH ligand was synthesised according to the previous method with some modifications (Amoroso et al. 1994). The $[\text{Re}(\text{PyPzH})(\text{CO})_3\text{Cl}]$ complex was prepared following literature method (Kianfar et al. 2015) from the reaction of pentacarbonylchlororhenium(I) (250 mg, 0.691 mmol) and PyPzH (110 mg, 0.760 mmol) ligand in toluene with a 1:1.1 ratio (Figure 1). This reaction mixture was brought to reflux under nitrogen atmosphere for about 5 h. The product

was obtained as a precipitate and washed with an excess *n*-hexane. The product was collected as a pale-yellow solid (243 mg, 78.0% yield; ESI-MS (acetone, $[m/z]$): 499).

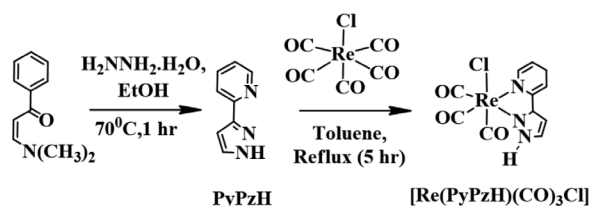


FIGURE 1. The synthetic route for $[\text{Re}(\text{PyPzH})(\text{CO})_3\text{Cl}]$

GENERAL INSTRUMENTATION

The infrared spectra of PyPzH and $[\text{Re}(\text{PyPzH})(\text{CO})_3\text{Cl}]$ were collected using an Agilent Cary 630 with a zinc selenide attenuated total reflectance sampling accessory in the range of $4000\text{--}400\text{ cm}^{-1}$. The proton (^1H) and carbon (^{13}C) NMR spectra were collected in a deuterated DMSO- d_6 at room temperature using Bruker 400 spectrometer. The mass-to-charge ratio (m/z) of gaseous PyPzH and Re(I) complex ions and its fragments were determined by Bruker Daltonic (MicroTOF Q) mass spectrometer (capillary potential - 4500 V; aerosol - 0.2 Bar; heat - 180°C). The electronic absorption (UV-Vis) analysis of the sample was measured with the UV-1650 PC SHIMADZU spectrophotometer. The single crystal X-ray diffraction data were collected on Bruker SMART APEX CCD.

COMPUTATIONAL METHODS

The coordinates of $[\text{Re}(\text{PyPzH})(\text{CO})_3\text{Cl}]$ from single-crystal x-ray diffraction analysis was extracted and used as an input for geometry optimisation via *ab-initio*, DFT. The electronic structure and UV-Vis absorption properties were subsequently studied with TDDFT. The Lee–Yang–Parr (B3LYP) exchange-correlation functional was used for the first-principle quantum calculation. The basis-set of 6-311++G (d, p) with polarization and diffuse functions was utilized for non-metals; while, the LAN2LDZ basis was considered as the effective core potential for rhenium (Becke 1993, 1988; Davidson & Feller 1986; Hehre et al. 1986; Lee et al. 1988). The vibrational frequency calculations were implemented and verified to ensure that only positive eigen values exist. The Tomasi's polarizable continuum model (PCM) was utilized in the calculation to model the solvent reaction field for acetonitrile ($\epsilon = 35.688$) (Cossi et al. 2003; Miertuš et al. 1981).

RESULTS AND DISCUSSION

INFRARED SPECTROSCOPY

Table 1 shows the stretching frequency of functional groups of PyPzH ligand and the corresponding rhenium

complex, $[\text{Re}(\text{PyPzH})(\text{CO})_3\text{Cl}]$. The PyPzH ligand showed the characteristic featured signals of N-H, C=N and C=C at 3264, 1592 and 1567 cm^{-1} , respectively. Upon coordination with the rhenium(I) metal ion, the infrared spectrum showed the stretching frequencies of $\nu(\text{N-H}) = 3137$, $\nu(\text{C=N}) = 1614$ and $\nu(\text{C=C}) = 1513$ cm^{-1} . In addition, the vibrational signals for C=O functional group were also detected in the 1860-2020 cm^{-1} region. The presence of $\nu(\text{C=O})$ in the IR spectrum ascertained the coordination of ligand with Re(I) metal centre. However, there were only two carbonyl signals observed. Among the three C=O present in the Re(I) complex, two of which are situated at the equatorial position in an octahedral geometry, while, the third C=O is essentially located at a right angle with respect to the other carbonyls. Therefore, the two carbonyls at the equatorial position are predicted to have similar stretching frequency and produced overlapping signals with identical wavenumbers. The presence of the tricarbonyl peaks is further investigated and confirmed by ^{13}C NMR spectroscopy.

TABLE 1. The infrared spectral data for the main functional groups of free PyPzH ligand and $[\text{Re}(\text{PyPzH})(\text{CO})_3\text{Cl}]$ complex

Functional group (stretching)	Wavenumber (cm^{-1})	
	PyPzH	$[\text{Re}(\text{PyPzH})(\text{CO})_3\text{Cl}]$
N-H	3264	3137
C=O	-	2018
	-	-
	-	1866
C=N	1592	1614
C=C	1567	1513

^{13}C AND ^1H (NMR) SPECTROSCOPY

The ^{13}C -NMR spectra for PyPzH and the corresponding rhenium complex, $[\text{Re}(\text{PyPzH})(\text{CO})_3\text{Cl}]$ showed the presence of eight and eleven carbon signals, respectively. The prominent feature found for the ^{13}C -NMR spectrum of $[\text{Re}(\text{PyPzH})(\text{CO})_3\text{Cl}]$ was the appearance of three signals in the region of 190.0-199.0 ppm. These signals are assigned to the tricarbonyl ligands of the complex. The rest of the carbon signals in the ^{13}C -NMR spectrum of Re(I) complex corresponded well to that of the free PyPzH ligand in terms of chemical shifts. In addition, the integration of ^1H -NMR signals was also congruent to the actual number of protons present in the ligand and complex. One of the notable signals present in the ^1H -NMR spectra was the appearance of a far downfield singlet for N-H signal at 13.15 ppm and 14.84 ppm for the ligand and Re(I) complex, respectively.

X-RAY CRYSTALLOGRAPHY

The single crystal structure of $[\text{Re}(\text{PyPzH})(\text{CO})_3\text{Cl}]$ molecule is shown in Figure 2 with one water molecule held by intramolecular hydrogen bond between O1W atom of water molecule with H7 atom of the pyrazole moiety

with a D \cdots A distance of 2.780 (8) Å and D-H \cdots A angle of 167°. This has given the crystal a molecular formula of $\text{C}_{11}\text{H}_7\text{ClN}_3\text{O}_3\text{Re}\cdot\text{H}_2\text{O}$. The crystal was crystallized from a mixture of dichloromethane/methanol solution through a slow evaporation technique. It is in a monoclinic system with C2/c space group. The crystal dimension is $a = 27.7422(14)$ Å, $b = 11.1456(5)$ Å, $c = 9.2461(4)$ Å, with $\alpha = 90^\circ$, $\beta = 92.552(2)^\circ$ and $\gamma = 90^\circ$ (Table 2). The three carbonyl ligands were at facial configuration, which is in agreement with the infrared data. The PyPzH ligand was coordinated to Re^I through the predicted N,N configuration with bond lengths of Re1-N1 and Re1-N2 measured to be 2.209(4) Å and 2.155(5) Å, respectively. This coordination formed a 5-membered chelating ring with a N1-Re1-N2 dihedral angle of 73.3(18)° (Table 3) which is in agreement with the chelating angle of other Re^I N,N heterocyclic ligand system (Kianfar et al. 2015; Piletska et al. 2015). In addition, the pyridine plane (N1/C4/C5/C6/C7/C8) and the pyrazole plane (N2/N3/C9/C10/C11) were nearly planar with a minor deviation angle of 3.1(3)° due to the restriction upon coordination with Re^I. The bond length of Re-Cl and Re-N of the pyridine and pyrazole groups are similar to the corresponding bond lengths in related structures (Obata et al. 2008; Seridi et al. 2011).

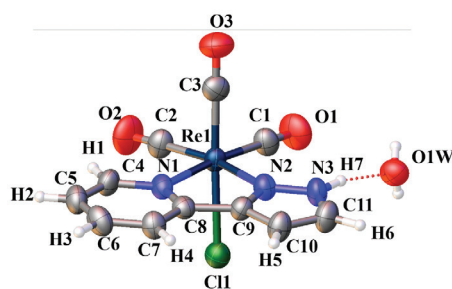


FIGURE 2. The molecular structure of $[\text{Re}(\text{PyPzH})(\text{CO})_3\text{Cl}]$. Displacement ellipsoids are drawn at the 50% probability level. Hydrogen bond is shown as dashed line

TABLE 2. Crystal data and structure refinement parameters for $[\text{Re}(\text{PyPzH})(\text{CO})_3\text{Cl}]$

Parameter	Data
Empirical formula	$\text{C}_{11}\text{H}_9\text{Cl}_1\text{N}_3\text{O}_4\text{Re}_1$
Formula weight	468.87
Temperature	307 K
Crystal system	Monoclinic
Space group	C2/c
Unit cell dimensions	$a = 27.7422(14)$ Å $b = 11.1456(5)$ Å $c = 9.2461(4)$ Å
Volume	$2856.1(2)$ Å ³
Z	8
Crystal size (mm)	0.26 x 0.09 x 0.07
θ range for data collection	2.9 - 28.3°
Final R_1 , wR_2	0.0395, 0.1149

ATOMIC CHARGES ANALYSIS

According to the Mulliken atomic charges, the highest positively charged atom is Re¹ (Figure 3). The positive and negative charges are an indication of their electron accepting and donating abilities. The rhenium atom is essentially charged (+1) and possesses a d^6 electron configuration with two available high-spin e_g orbitals namely $d(x^2-y^2)$ and $d(z^2)$. The next three atoms with high positive charges are H7, N2 and N1. While, the three atoms with high negative charges are C6, N3 and C11. The highly negative N3 atom attracts significant electron density from the attached H7 atom, as a result, H7 is more positively charged compared to the other hydrogen atoms bonded to the carbon atoms. In fact, H7 was observed to form hydrogen bonding with a water solvate in the crystal lattice. Interestingly, among the three nitrogen atoms available only N3 atom is negatively charged ascertaining the role of the PyPzH ligand as an electron acceptor. The diimine ligands are known to engage as a π -acceptor with

metal centres (Pearce et al. 2017). However, the negatively charged N3 atom may counterbalance the positive charges induced by neighbouring N2 atom. Therefore, a disparity in electron distribution is expected to occur between the pyridine and pyrazole moieties. It is also observed that the three carbonyls and the chlorine atom are negatively charged, acting as donors; while, the PyPzH may accept the delocalisation of electron from the metal centre via N1 and N2 atoms. As per argument, in order to tune the bandgap for optimum visible to near-infrared sensitivity, the energy of the empty states located at the PyPzH ligand should be lowered yet retain the HOMO for maximum oxidation ability.

ELECTRONIC ABSORPTION INVESTIGATION

The experimental and TDDFT calculated UV-Vis data including maximum wavelength (λ_{max}), optical bandgap (E_g), extinction coefficient (ϵ), oscillator strengths

TABLE 3. Geometric parameters of selected bond lengths (Å) and angle (°) for [Re(PyPzH)(CO)₃Cl]

Bond	Length (Å)	Angle	Degree (°)
Re1-Cl4	2.4917(14)	N1-Re1-N2	73.3(18)
Re1-N1	2.209(4)	N1-Re1-C2	96.1(2)
Re1-N2	2.155(5)	N1-Re1-C3	94.0(2)
N2-N3	1.341(8)	N2-Re1-C1	101.8(2)
N2-C9	1.346(7)	N2-Re1-C3	93.7(2)
N3-C11	1.342(10)		
N1-C4	1.361(8)		
N1-C8	1.337(7)		
O1-C1	1.144(7)		
O2-C2	1.139(9)		
O3-C3	1.159(8)		

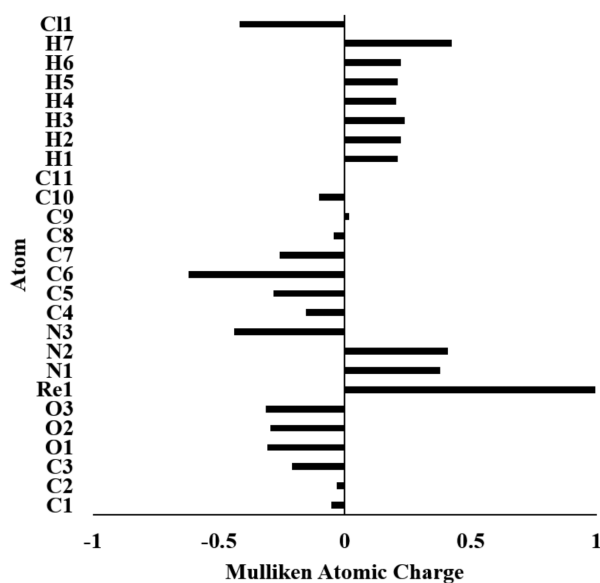


FIGURE 3. Mulliken atomic charge distribution for the optimised [Re(PyPzH)(CO)₃Cl] structure with the labelled atoms according to Figure 2

(f), predominant transitions and orbitals involved are shown in Table 4. The experimental UV-Vis spectrum of $[\text{Re}(\text{PyPzH})(\text{CO})_3\text{Cl}]$ measured in acetonitrile displayed three discernible absorption bands with increasing intensities: A-C (Figure 4(A)). Likewise, the theoretically calculated UV-Vis spectrum also depicted three similar absorption bands with the same solvent reaction field consideration. Besides, the calculated absorption band A and C is slightly shifted bathochromically (red-shifted) and hypsochromically (blue-shifted), respectively, with regards to the experimental UV-Vis spectrum. Nevertheless, the calculated spectrum with Gaussian-type distribution has demonstrated similar spectral shape and profile in terms of relative intensities for the three dominant bands. The TDDFT calculations based on B3LYP hybrid function are notable to over-estimate bandgap energies (Fui et al. 2016).

Figure 5 depicts the first six frontier molecular orbitals of $[\text{Re}(\text{PyPzH})(\text{CO})_3\text{Cl}]$. The initial lowest energy absorption band (A) is experimentally recorded at $\lambda_{\text{max}} = 331$ with a relatively low extinction coefficient, $\epsilon = 0.467 \times 10^4 \text{ M}^{-1}\text{cm}^{-1}$ and was ascribed to the HOMO-1 \rightarrow LUMO transition. This transition corresponded to the MLCT band with the photoexcited electron in the singlet state. Typically, the lowest energy photoexcitation of electron should involve the filled molecular orbitals of HOMO and yet, in this case, it involves the second lowest filled

molecular orbitals (HOMO-1). Both, HOMO and HOMO-1 are predominantly found on the $d\pi$ -orbitals of rhenium centre as well as on the Cl and CO which are located in a *trans* configuration to each other along the z -axis. However, the filled $d\pi$ -orbitals (Re) of HOMO are situated in the yz -plane together with the π -orbitals of Cl and CO, while, the HOMO-1 involved the same moieties but different molecular orbitals in the xz -plane. The HOMO-1 has the same orientation as the anti-orbital (π^*) of LUMO which facilitates a better overlapping of corresponding orbitals and pave the way for the MLCT process to occur efficiently.

The next higher energy absorption band (B) is detected at 292 nm ($\epsilon = 4.24 \times 10^4 \text{ M}^{-1}\text{cm}^{-1}$). Based on TDDFT calculations, two dominant electronic transitions are involved in this band namely HOMO-3 \rightarrow LUMO ($f = 0.1258$) and HOMO-4 \rightarrow LUMO ($f = 0.1092$). Both of which are ascribed to the ligand-based $\pi \rightarrow \pi^*$ molecular orbitals. Comparatively, the former has a higher oscillator strength. The HOMO-3 and LUMO are concurrently located on the PyPzH ligand and the disparity of electronic distribution between the Py and PzH fragments allows for a lower energy photoexcitation of electrons. Absorption band C has the highest vertical electron excitation intensity at $\lambda_{\text{max}} = 227$ ($\epsilon = 5.46 \times 10^4 \text{ M}^{-1}\text{cm}^{-1}$). The electronic transition involves the Cl atom (HOMO-7) to the three available carbonyls ligands (LUMO+3). Upon photoexcitation, the ground state electrons of Cl atom populate the rhenium

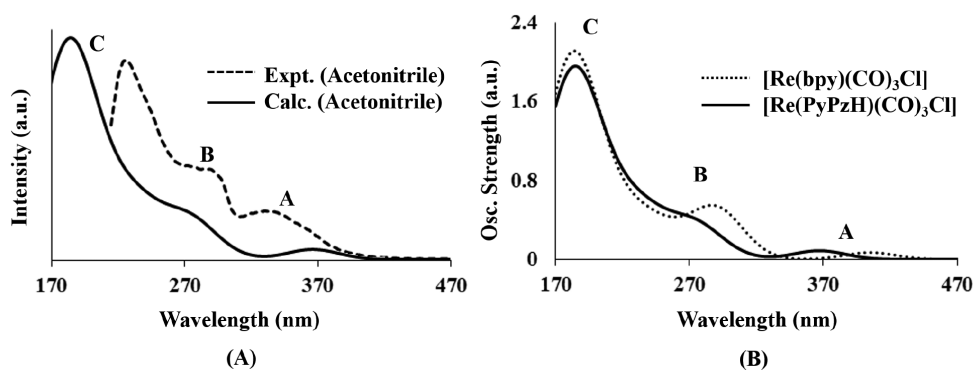


FIGURE 4. (A) Experimental (dashed line) and DFT calculated (solid line) UV-Vis spectra (acetonitrile) of $[\text{Re}(\text{PyPzH})(\text{CO})_3\text{Cl}]$; (B) Comparison of calculated UV-Vis spectra (acetonitrile) of $[\text{Re}(\text{PyPzH})(\text{CO})_3\text{Cl}]$ and $[\text{Re}(\text{bpy})(\text{CO})_3\text{Cl}]$ with prominent absorption bands labelled as A-C

TABLE 4. Experimental and calculated UV-Vis excitation data of $[\text{Re}(\text{PyPzH})(\text{CO})_3\text{Cl}]$ recorded in acetonitrile

Band	Expt.			TDDFT/B3LYP			Key transitions and character ^c
	λ_{max}^a (nm)	E_g^b (eV)	ϵ^a	λ_{max}^a (nm)	E_g^b (eV)	Osc. ^a (f)	
A	331	3.74	0.467	367	3.38	0.0866	(96%) HOMO-1 _(Re+Cl+aCO) \rightarrow LUMO _(PyPzH)
B	292	4.24	0.853	281	4.41	0.1258	(67%) HOMO-3 _(PyPzH) \rightarrow LUMO _(PyPzH)
C	227	5.46	1.942	179	6.92	0.1650	(60%) HOMO-4 _(Cl+PzH) \rightarrow LUMO _(PyPzH) (17%) HOMO-7 _(Cl) \rightarrow LUMO+3 _(3CO)

^a $\lambda_{\text{max}}/\text{nm}$, ($\epsilon \times 10^4 \text{ M}^{-1}\text{cm}^{-1}$); $2 \times 10^{-5} \text{ M}$; Osc. = Oscillator Strength

^b $E_g = 1239.5/\lambda_{\text{max}}$ (Fui et al. 2012b; Mark-Lee et al. 2013)

^c Re = $d\pi$ (Rhenium), Cl = chlorine atom, aCO = axial carbonyl, 3CO = all three carbonyls are involved, PzH = pyrazole fragment

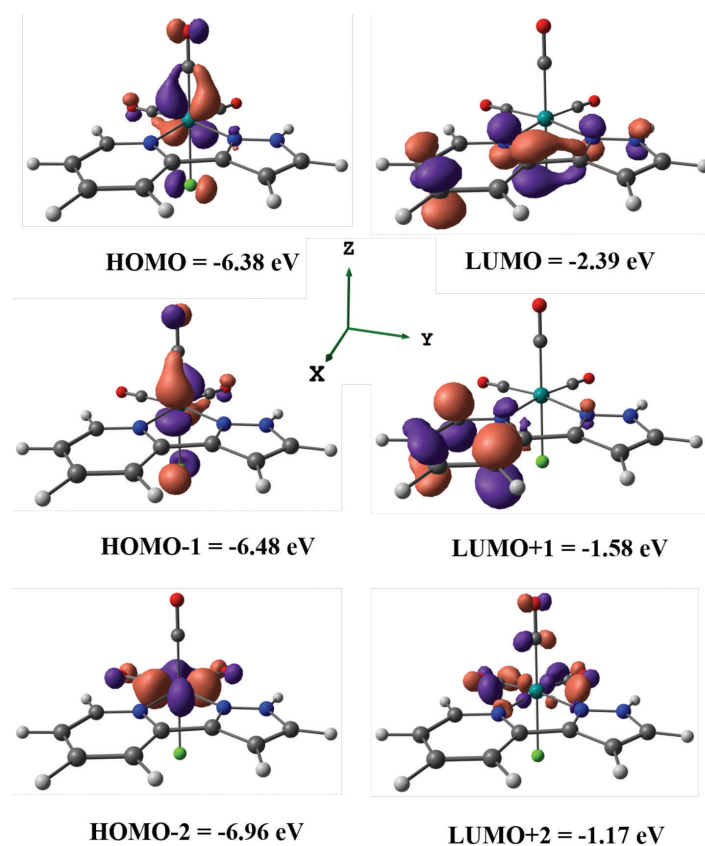


FIGURE 5. Illustration (contour value = 0.075) of frontier HOMOs and LUMOs for $[\text{Re}(\text{PyPzH})(\text{CO})_3\text{Cl}]$

centre and flows to the carbonyl via π -back bonding. This observation is also common in the organometallic chemistry of transition metals with multi-atomic ligands such as nitrosyl (Fui et al. 2012a; Wun et al. 2013).

For the purpose of comparison, the TDDFT UV-Vis spectrum of $[\text{Re}(\text{bpy})(\text{CO})_3\text{Cl}]$ was established and Figure 4(B) shows the comparison of TDDFT calculated UV-Vis spectra for $[\text{Re}(\text{PyPzH})(\text{CO})_3\text{Cl}]$ and $[\text{Re}(\text{bpy})(\text{CO})_3\text{Cl}]$. The $[\text{Re}(\text{bpy})(\text{CO})_3\text{Cl}]$ analogue has similar geometrical and structural properties with respect to $[\text{Re}(\text{PyPzH})(\text{CO})_3\text{Cl}]$. As mentioned earlier, the $[\text{Re}(\text{bpy})(\text{CO})_3\text{Cl}]$ has been evaluated alongside newly synthesised Re(I) complexes as a standard reference point. It is observed that band A and B of $[\text{Re}(\text{bpy})(\text{CO})_3\text{Cl}]$ were noticeably red-shifted compared to $[\text{Re}(\text{PyPzH})(\text{CO})_3\text{Cl}]$. This observation is comprehensible since the only structural difference between the two analogous complexes involved the diimine ligands where the LUMO is found and only band A and B are predicted to engage LUMO as the receiving empty molecular orbital (Table 4). The PyPzH ligand is known to have a relative higher-lying π^* orbital compared with that of bpy and hence lower energy is required for the photoexcitation of electrons in $[\text{Re}(\text{bpy})(\text{CO})_3\text{Cl}]$ (Klein et al. 2011). The photocatalytic activity of Re(I) complexes are typically enhanced with extended light absorption towards the visible and near-infrared region. Nevertheless, the $[\text{Re}(\text{PyPzH})(\text{CO})_3\text{Cl}]$

can be used as a precursor and undergo further structural manipulation involving the deprotonation of an acidic N-H proton from the pyrazole moiety (Mark-Lee et al. 2017).

ENTHALPY INVESTIGATION

In this study, the initial photocatalytic reduction of CO_2 involves the formation of OERS of Re(I) complexes and the successive dissociation of Cl atom. In view of this, a preliminary photocatalytic activity assessment of the synthesised Re(I) complex was conducted by considering the enthalpy of reaction ($\Delta H_{\text{rxn}}^\circ$) for Cl dissociation (1) along with that of $[\text{Re}(\text{bpy})(\text{CO})_3\text{Cl}]$. The complete and balanced reaction equation for the Cl^- dissociation from $[\text{Re}(\text{PyPzH})(\text{CO})_3\text{Cl}]^{\bullet-}$ is given in Figure 6. The enthalpy data of the related species are recorded in Table 5. The dissociation of Cl^- from the OERS, $[\text{Re}(\text{PyPzH})(\text{CO})_3\text{Cl}]^{\bullet-}$ ($\Delta H_{\text{rxn}}^\circ = +131.28$ kJ/mol) required approximately lesser than two-thirds of the energy associated with that of $[\text{Re}(\text{bpy})(\text{CO})_3\text{Cl}]^{\bullet-}$ ($\Delta H_{\text{rxn}}^\circ = +210.04$ kJ/mol). The energy difference between both calculated enthalpies is $\Delta 78.76$ kJ/mol. These results suggested that the $[\text{Re}(\text{PyPzH})(\text{CO})_3\text{Cl}]$ complex may have an advantage over the benchmark $[\text{Re}(\text{bpy})(\text{CO})_3\text{Cl}]$ complex with regards to the initial photocatalytic CO_2 reduction step. Besides, the versatile $[\text{Re}(\text{PyPzH})(\text{CO})_3\text{Cl}]$ provides a

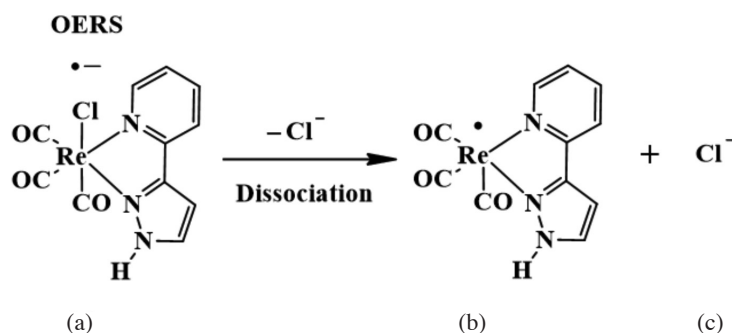


FIGURE 6. The dissociation of Cl atom from the OERS of $[\text{Re}(\text{PyPzH})(\text{CO})_3\text{Cl}]$

TABLE 5. DFT calculated enthalpy data

$\Sigma H^{\circ}(\text{a})$	$\Sigma H^{\circ}(\text{b+c})$	$\Delta H^{\circ}_{\text{rxn}} = \Sigma H^{\circ}(\text{b+c}) - \Sigma H^{\circ}(\text{a})$
Hartree		(kJ/mol)
$[\text{Re}(\text{PyPzH})(\text{CO})_3\text{Cl}]^{\bullet-}$ = -1352.92	$[\text{Re}(\text{PyPzH})(\text{CO})_3]^{\bullet} + \text{Cl}^-$ = -1352.87	+131.28
$[\text{Re}(\text{bpy})(\text{CO})_3\text{Cl}]^{\bullet-}$ = -1375.01	$[\text{Re}(\text{bpy})(\text{CO})_3]^{\bullet} + \text{Cl}^-$ = -1374.93	+210.04

facile structural modification on the π -accepting ligand via the amine proton of the pyrazole moiety and directly enables the fine tuning of bandgap energy.

$$\Delta H^{\circ}_{\text{rxn}} = \Sigma H^{\circ}(\text{products}) - \Sigma H^{\circ}(\text{reactant}) \quad (1)$$

CONCLUSION

A new Re(I) tricarbonyl complex with 2-(1H-pyrazol-3-yl)pyridine, $[\text{Re}(\text{PyPzH})(\text{CO})_3\text{Cl}]$, was successfully synthesised and characterised. The complex crystallised in a monoclinic system with C2/c space group. The MLCT band of $[\text{Re}(\text{PyPzH})(\text{CO})_3\text{Cl}]$ complex was comparatively blue-shifted with respect to the benchmark $[\text{Re}(\text{bpy})(\text{CO})_3\text{Cl}]$ complex based on 2,2'-bipyridine ligand. The former is known to have a relatively destabilised π^* -molecular orbital compared to the latter due to the higher energy of the pyrazole moiety. On the other hand, $[\text{Re}(\text{PyPzH})(\text{CO})_3\text{Cl}]$ was thermodynamically more favourable compared to $[\text{Re}(\text{bpy})(\text{CO})_3\text{Cl}]$ based on the preliminary assessment of photocatalytic CO_2 reduction. The $[\text{Re}(\text{PyPzH})(\text{CO})_3\text{Cl}]$ requires a lower energy for the dissociation of Cl in the initial step of the photocatalytic CO_2 reduction. Thus, the lower extension to the visible light absorption for the MLCT experienced by $[\text{Re}(\text{PyPzH})(\text{CO})_3\text{Cl}]$ is compensated in terms of the mechanical feasibility involving the photocatalytic cycle. Hence, $[\text{Re}(\text{PyPzH})(\text{CO})_3\text{Cl}]$ is a promising precursor photocatalyst and provides the versatility of molecular modification for further optimisation of the photocatalytic properties.

ACKNOWLEDGEMENTS

The authors thank the Ministry of Higher Education, Malaysia for ERGS/1/2013/TK07/UKM/02/2 research grant and MyPhD support for CYY, the Ministry of Science, Technology and Innovation for 06-01-02-SF1001 research grant and Universiti Kebangsaan Malaysia for DIP-2016-026 research grant. Many thanks to Prof. Hideaki Kasai, Prof. Wilson Agerico Diño and Osaka University (Japan) for supporting us with quantum computational facilities. We are grateful to the School of Chemical Sciences and Food Technology, Faculty of Science and Technology and Fuel Cell Institute (UKM) for their provision of experimental facilities.

REFERENCES

- Agarwal, J., Johnson, R.P. & Li, G. 2011. Reduction of CO_2 on a tricarbonyl rhenium(I) complex: Modeling a catalytic cycle. *Journal of Physical Chemistry A* 115(13): 2877-2881.
- Amoroso, A.J., Thompson, A.M.C., Jeffery, J.C., Jones, P.L., McCleverty, J.A. & Ward, M.D. 1994. Synthesis of the new tripodal ligand tris-[3-(2'-pyridyl)pyrazol-1-yl] hydroborate, and the crystal structure of its europium(III) complex. *Journal of the Chemical Society, Chemical Communications* 24: 2751-2752.
- Becke, A.D. 1988. Density-functional exchange-energy approximation with correct asymptotic behaviour. *Physical Review A* 38(6): 3098-3100.
- Becke, A.D. 1993. Density functional thermochemistry III the role of exact exchange. *Journal of Chemical Physics* 98: 5648-5652.
- Chou, P.T. & Chi, Y. 2006. Osmium- and ruthenium-based phosphorescent materials: Design, photophysics, and utilization in OLED fabrication. *European Journal of Inorganic Chemistry* 17: 3319-3332.

- Cossi, M., Rega, N., Scalmani, G. & Barone, V. 2003. Molecules in solution with the C-PCM solvation model. *Journal of Computational Chemistry* 24(6): 669-681.
- Davidson, E.R. & Feller, D. 1986. Basis set selection for molecular calculations. *Chemical Reviews* 86(4): 681-696.
- Doherty, M.D., Grills, D.C. & Fujita, E. 2009. Synthesis of fluorinated ReCl(4,4'-R₂-2,2'-bipyridine)(CO)₃ complexes and their photophysical characterization in CH₃CN and supercritical CO₂. *Inorganic Chemistry* 48(5): 1796-1798.
- Fui, M.L.W., Hang, N.K., Arifin, K., Minggu, L.J. & Kassim, M.B. 2016. Photocatalytic degradation of bromothymol blue with Ruthenium(II) bipyridyl complex in aqueous basic solution. *AIP Conference Proceedings* 1784(II): 1-6.
- Fui, M.L.W., Hang, N.K., Minggu, L.J., Umar, A.A. & Kassim, M.B. 2012a. Determination of band energy levels for tungsten nitrosyldithiolene. *Sains Malaysiana* 41(4): 439-444.
- Fui, M.L.W., Minggu, L.J. & Kassim, M.B. 2012b. Photochemical properties of molybdenum dithiolene. *Sains Malaysiana* 41(5): 597-601.
- Gibson, D.H. & He, H. 2001. Synthesis and properties of *fac*-Re(dmbpy)(CO)₃CHO (dmbpy = 4,4[prime or minute]-dimethyl-2,2[prime or minute]-bipyridine), a possible intermediate in reductions of CO₂ catalyzed by *fac*-Re(dmbpy)(CO)₃Cl. *Chemical Communications* (20): 2082-2083.
- Hawecker, J., Lehn, J.M. & Ziessel, R. 1983. Combinations as homogeneous catalysts. *Chemical Communications* 536: 536-538.
- Hehre, W.J., Radom, L., Schleyer, P.V.R. & Pople, J.A. 1986. *Ab initio* molecular orbital theory. *Accounts of Chemical Research* 9: 399-406.
- Kianfar, E., Kaiser, M. & Knör, G. 2015. Synthesis, characterization and photoreactivity of rhenium and molybdenum carbonyl complexes with iminopyridine ligands. *Journal of Organometallic Chemistry* 799-800: 13-18.
- Klein, C., Baranoff, E., Grätzel, M. & Nazeeruddin, M.K. 2011. Convenient synthesis of tridentate 2,6-di(pyrazol-1-yl)-4-carboxypyridine and tetradentate 6,6'-di(pyrazol-1-yl)-4,4'-dicarboxy-2,2'-bipyridine ligands. *Tetrahedron Letters* 52(5): 584-587.
- Komala, T. & Khun, T.C. 2014. Biological carbon dioxide sequestration potential of *Bacillus pumilus*. *Sains Malaysiana* 43(8): 1149-1156.
- Lee, C., Yang, W. & Parr, R. 1988. Development of the Colle-Salvetti correlation energy formula into a functional of the electron density. *Physical Review B* 37(2): 785-789.
- Mark-Lee, W.F., Rusydi, F., Minggu, L.J. & Kassim, M.B. 2017. Bis(Bipyridyl)-Ru(II)-1-benzoyl-3-(pyridine-2-yl)-1H-pyrazole as potential photosensitizer: Experimental and density functional theory study. *Jurnal Teknologi* 79(5-3): 117-123.
- Mark-Lee, W.F., Ng, K.H., Minggu, L.J., Umar, A.A. & Kassim, M.B. 2013. A molybdenum dithiolene complex as a potential photosensitizer for photoelectrochemical cells. *International Journal of Hydrogen Energy* 38(22): 9578-9584.
- Miertuš, S., Scrocco, E. & Tomasi, J. 1981. Electrostatic interaction of a solute with a continuum. A direct utilization of *Ab initio* molecular potentials for the prevision of solvent effects. *Chemical Physics* 55(1): 117-129.
- Ng, K.H., Minggu, L.J., Mark-Lee, W.F., Arifin, K., Jumali, M.H.H. & Kassim, M.B. 2018. A new method for the fabrication of a bilayer WO₃/Fe₂O₃ photoelectrode for enhanced photoelectrochemical performance. *Materials Research Bulletin* 98: 47-52.
- Ng, K.H., Minggu, L.J., Jaafar, N.A., Arifin, K. & Kassim, M.B. 2017. Enhanced plasmonic photoelectrochemical response of Au sandwiched WO₃ photoanodes. *Solar Energy Materials and Solar Cells* 172: 361-367.
- Ng, K.H., Minggu, L.J., Jumali, M.H.H. & Kassim, M.B. 2012. Nickel-doped tungsten trioxide photo electrodes for photoelectrochemical water splitting reaction. *Sains Malaysiana* 41(7): 893-899.
- Obata, M., Kitamura, A., Mori, A., Kameyama, C., Czaplewski, J.A., Tanaka, R., Kinoshita, I., Kusumoto, T., Hashimoto, H., Harada, M., Mikata, Y., Funabiki, T. & Yano, S. 2008. Syntheses, structural characterization and photophysical properties of 4-(2-pyridyl)-1,2,3-triazole rhenium(I) complexes. *Dalton Transactions* 25: 3292-3300.
- Pearce, B.H., Ogotu, H.F. & Luckay, R.C. 2017. Synthesis of pyrazole-based pyridine ligands and their use as extractants for nickel(II) and copper(II): Crystal structure of a copper(II)-ligand complex. *European Journal of Inorganic Chemistry* 2017(8): 1189-1201.
- Piletska, K.O., Domasevitch, K.V., Gusev, A.N., Shul'gin, V.F. & Shtemenko, A.V. 2015. *fac*-Tricarbonyl rhenium(I) complexes of triazole-based ligands: Synthesis, X-ray structure and luminescent properties. *Polyhedron* 102(1): 699-704.
- Radaideh, J.A., Alazba, A.A., Amin, M.N., Shatnawi, Z.N. & Amin, M.T. 2016. Improvement of indoor air quality using local fabricated activated carbon from date stones. *Sains Malaysiana* 45(1): 59-69.
- Sahara, G. & Ishitani, O. 2015. Efficient photocatalysts for CO₂ reduction. *Inorganic Chemistry* 54(11): 5096-5104.
- Seridi, A., Wolff, M., Boulay, A., Saffon, N., Coulais, Y., Picard, C., MacHura, B. & Benoist, E. 2011. Rhenium(I) and technetium(I) complexes of a novel pyridyltriazole-based ligand containing an arylpiperazine pharmacophore: Synthesis, crystal structures, computational studies and radiochemistry. *Inorganic Chemistry Communications* 14(1): 238-242.
- Tamaki, Y. & Ishitani, O. 2017. Supramolecular photocatalysts for the reduction of CO₂. *ACS Catalysis* 7(5): 3394-3409.
- Wun, F.M.L., Pui, L.K., Heng, L.Y. & Kassim, M. 2013. Molybdenum complex as potential photosensitizer for direct water splitting. *Materials Science Forum* 756: 231-237.
- Yamazaki, Y., Takeda, H. & Ishitani, O. 2015. Photocatalytic reduction of CO₂ using metal complexes. *Journal of Photochemistry and Photobiology C: Photochemistry Reviews* 25: 106-137.
- Yilmaz, F., Balta, M.T. & Selbaş, R. 2016. A review of solar based hydrogen production methods. *Renewable and Sustainable Energy Reviews* 56: 171-178.
- Wun Fui Mark-Lee, Yan Yi Chong, Kung Pui Law, Ishak B. Ahmad & Mohammad B. Kassim*
School of Chemical Sciences and Food Technology
Faculty of Science and Technology
Universiti Kebangsaan Malaysia
43600 UKM Bangi, Selangor Darul Ehsan
Malaysia

Mohammad B. Kassim*
Institut Sel Fuel
Universiti Kebangsaan Malaysia
43600 UKM Bangi, Selangor Darul Ehsan
Malaysia

Kung Pui Law
School of Biosciences
No. 1 Jalan Taylor's
47500 Subang Jaya, Selangor Darul Ehsan
Malaysia

*Corresponding author; email: mb_kassim@ukm.edu.my

Received: 17 September 2017

Accepted: 28 February 2018